The dynamics of Br(^2P_j) formation in the photodissociation of vinyl and perfluorovinyl bromides

Kyoung-Seok Lee, Keon Woo Lee, Tae Kyu Kim, Ryong Ryoo, and Kyung-Hoon Jung[a)]
Department of Chemistry and School of Molecular Science (BK21), Korea Advanced Institute of Science and Technology, Daeduck Science Town, Daejeon 305-701, Korea

(Received 16 August 2004; accepted 8 October 2004; published online 3 January 2005)

The photodissociation dynamics of vinyl bromide and perfluorovinyl bromide have been investigated at 234 nm using a photofragment ion imaging technique coupled with a state-selective [2+1] resonance-enhanced multiphoton ionization scheme. The nascent Br atoms stem from the primary C–Br bond dissociation leading to the formation of $C_2H_3(\tilde{X})$ and Br(^2P_j; $j=1/2,3/2$). The obtained translational energy distributions have been well fitted by a single Boltzmann and three Gaussian functions. Boltzmann component has not been observed in the perfluorovinyl bromide. The repulsive $^3A'(n,\sigma^*)$ state has been considered as the origin of the highest Gaussian components. Middle translational energy components with Gaussian shapes are produced from the $^1A''(\pi,\sigma^*)$ and/or $^3A''(\pi,\sigma^*)$ which are very close in energy. Low-energy Gaussian components are produced via predissociation from the $^3A'(\pi,\pi^*)$ state. The assignments have also been supported by the recoil anisotropy corresponding to the individual components. It is suggested that intersystem crossing from the triplet states to the ground state has been attributed to the Boltzmann component and the fluorination reduces the probability of this electronic relaxation process. [DOI: 10.1063/1.1825994]

I. INTRODUCTION

Recently, many experimental and theoretical efforts have been made to investigate the photodissociation dynamics of organic molecules having C–X (X=Cl, Br, and I) bonds in the ultraviolet (UV) region.[1–5] Most studies have focused particularly upon the mechanism of the formation of X atoms in its ground ($^2P_{3/2}$) and excited ($^2P_{1/2}$) spin–orbit states because C–X bond fission following the absorption of ultraviolet light is one of well-known processes generating halogen atoms in the stratosphere that initiate and propagate ozone-depleting reactions.[6,7]

In the case of alkyl halides, diffuse absorption continua at short UV wavelengths are characteristic of repulsive excited states.[8–11] They originate from $\sigma^*\leftarrow n$ type electronic transitions localized on C–X bonds resulting in prompt dissociation. Detailed dynamics related to state-selective photodissociation and nonadiabatic interaction among potential-energy surfaces have been elucidated based on the energy distributions, recoil anisotropy parameters, and relative quantum yields of nascent X atoms.[1,2,12] When an organic halide contains another chromophore such as C=C and C=O moieties, dynamics become more complicated. For example, a $\pi^*\leftarrow\pi$ transition localized on C=C bond mainly contributes to the UV absorption of vinyl chloride.[13] At 193 nm, vinyl chloride becomes excited to a bound state, and Cl atoms are produced via curve-crossings to repulsive states and via an internal conversion process to the ground state.[14–22] It has been found that allyl chloride undergoes a photodissociation process similar to that of vinyl chloride.[23,24]

In comparison with vinyl chloride, vinyl bromide has received less attention although studies on its photodissociation may provide an opportunity to understand the effects of either mass or spin–orbit coupling energy. In its UV absorption spectrum, C–Br bond is responsible for considerable UV absorption as well as C=C, and a shoulder appears in the long wavelength region. This may imply that the two chromophores interact with each other.[25,26] Its photodissociation dynamics in this region, therefore, seems interesting, but recent studies have concentrated upon the dynamics near 200 nm, the absorption maximum.[27–29]

In this work, the photodissociation dynamics of vinyl bromide (C_2H_3Br) and perfluorovinyl bromide (C_2F_3Br) at 234 nm have been investigated. The nascent Br($^2P_{3/2}$) and Br*($^2P_{1/2}$) atoms were state-selectively detected via a [2+1] resonance-enhanced multi-photon ionization (REMPI) scheme and the photofragment ion-imaging technique. The translational energy distributions, recoil anisotropies, and relative quantum yields were extracted and interpreted to understand the potential energy surfaces and the interaction among them. The experimental findings in this work, together with our previous work on alkyl, allyl, acetyl halide systems, will apply to the more complicated systems such as benzene halides.

II. EXPERIMENT

The details of the experimental setup employed in this study has been described in our previous article.[30,31] In brief, our velocity mapping apparatus consists of a supersonic molecular beam source, a time-of-flight (TOF) mass spectrom-

[a)]Author to whom correspondence should be addressed. Electronic mail: khjung@kaist.ac.kr

eter, and a position-sensitive detector. 1.4% of C_2H_3Br (Aldrich, 98%) and C_2F_3Br (PCR, 97%) were seeded in He and introduced into a source chamber through a molecular beam valve (General Valve) with an orifice diameter of 800 μm. The total stagnation pressure was maintained at ~1.4 atm. The chamber was pumped with an oil diffusion pump (Alcatel, 6250). The pressure inside of the chamber was $\sim 10^{-5}$ Torr. The operation of the valve was synchronized with laser pulses at 10 Hz. After passing through a skimmer, the molecular beam was collimated by a pinhole with a diameter of 1 mm and then intersected the laser beam at a right angle.

The 355 nm output of a pulsed Nd:YAG laser (Spectra Physics, GCR-170) was used to pump a dye laser (Lumonics, HD500). An automated phase-matching system (Lumonics, HT-1000) was used for frequency-doubling to generate linearly polarized UV laser light. It was focused into an ionization region by a plano-convex lens with a focal length of 250 mm. It photolyzed C_2H_3Br and C_2F_3Br to produce $Br(^2P_{3/2})$ and $Br^*(^2P_{1/2})$, which were selectively ionized using [2+1] REMPI schemes at 233.69 and 234.02 nm via $6p\,^4P_{3/2}$ and $6p\,^4D_{1/2}$ intermediate states, respectively. Resultant Br ion clouds were accelerated using a repeller, an open extractor, and a ground electrode. The nonhomogeneous electric field caused around the electrodes functioned as an electrostatic ion lens[32] to create an image on a two-dimensinal position-sensitive detector that was composed of a dual-chevron microchannel plate (MCP), a phosphor screen (Galileo, FM3040), an image intensifier (Stanford Computer Optics, Quantum leap 5 n), and a charge-coupled device camera (Photometrics, CH250). A synchronously triggering pulse was applied to the image intensifier in order to segregate Br ion signals from background noises caused by scattering light and ions with different masses. More than 10^4 shots were integrated to construct an image at a personal computer. Time-of-flight mass spectra were collected using a photomultiplier tube (Hamamatsu, 1P21) and a digital oscilloscope (Lecroy 9310) instead of the image intensifier and the CCD camera. To minimize background noises, images and spectra obtained at off-resonance wavelengths under the same condition were subtracted from those at resonance wavelengths. All the images and spectra were averaged over a range of ≈4 cm^{-1} to cover all velocity components of Br atoms.

III. RESULTS AND ANALYSIS

Figure 1 shows the raw images corresponding to Br and Br* resulting from the photolysis of C_2H_3Br and C_2F_3Br (for details, refer to the caption). Each raw image is the two-dimensional (2D) projection of a three-dimensional (3D) velocity distribution with cylindrical symmetry around the polarization axis of laser light. The shape of an image, therefore, contains information on the speed and angular distribution of fragments. A three-dimensional velocity distribution is reconstructed from a raw image by performing an inverse Abel transformation. The cylindrical symmetry of a velocity distribution allows one to reconstruct a three-dimensional image from every slice containing the symmetry axis. Each raw image was smoothed, using a Gaussian filter with a 5×5 window and a standard deviation of 2 in pixel units so that noise effect that may arise during the transformation was reduced.

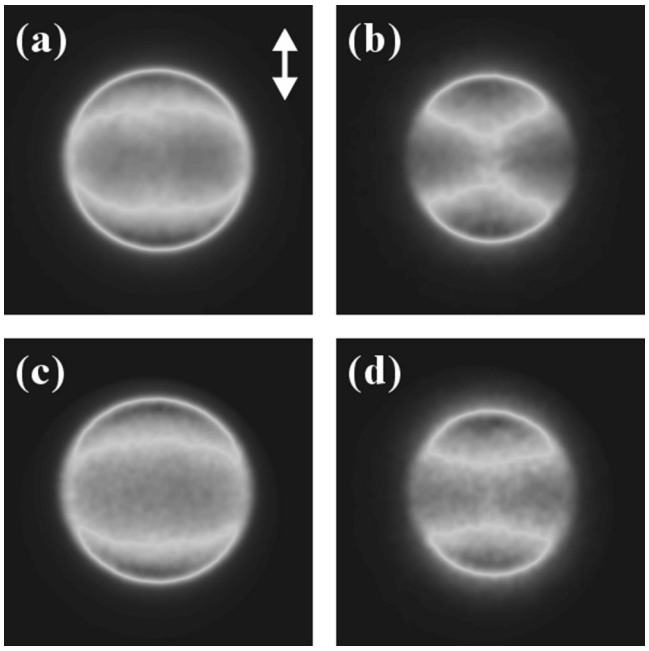

FIG. 1. Raw images of (a) Br and (b) Br* from C_2H_3Br. Those of Br and Br* from C_2F_3Br are shown in (c) and (d), respectively. In all images the linear polarization vector of the photolysis laser is vertical.

The angular distribution can be obtained by integrating the reconstructed 3D speed distribution over a proper range of speed at each angle. The translational anisotropy parameter, β, is extracted by fitting the ion signal intensity, $I(\theta)$, with a standard form

$$I(\theta) = C_{\mathrm{Norm}}(1 + \beta P_2(\cos\theta)), \tag{1}$$

where θ is the angle between the recoil velocity vector of fragments and the polarization axis of the photolysis laser. $P_2(\theta)$ is the second-order Legendre polynomial. C_{Norm} is a normalization factor. β varies from 2 for the limit of a parallel transition and to -1 for that of a perpendicular transition. As shown in Fig. 2, the anisotropy parameters determined for the overall ranges of velocity distributions are $\beta_{\mathrm{Br}} = 0.58 \pm 0.03$ and $\beta_{\mathrm{Br}^*} = 1.13 \pm 0.04$ for C_2H_3Br. For C_2F_3Br, $\beta_{\mathrm{Br}} = 0.53 \pm 0.05$, and $\beta_{\mathrm{Br}^*} = 0.77 \pm 0.08$. The values that deviate from the limits can result from different origins such as the long lifetime of the excited state, predissociation, and deviation of the recoil axis from the transition dipole moment. It can also be inferred that they are due to multiple channels contributing to the generation of Br and Br*. This is also supported by the total translational energy distributions of fragments that are characterized by several components (*vide infra*).

The total translational energy distribution based on a center-of-mass coordinate, $P(E_T)$, is obtained by converting the speed distribution, $P(v)$, according to the equations

$$P(E_T)dE = P(v)dv, \tag{2}$$

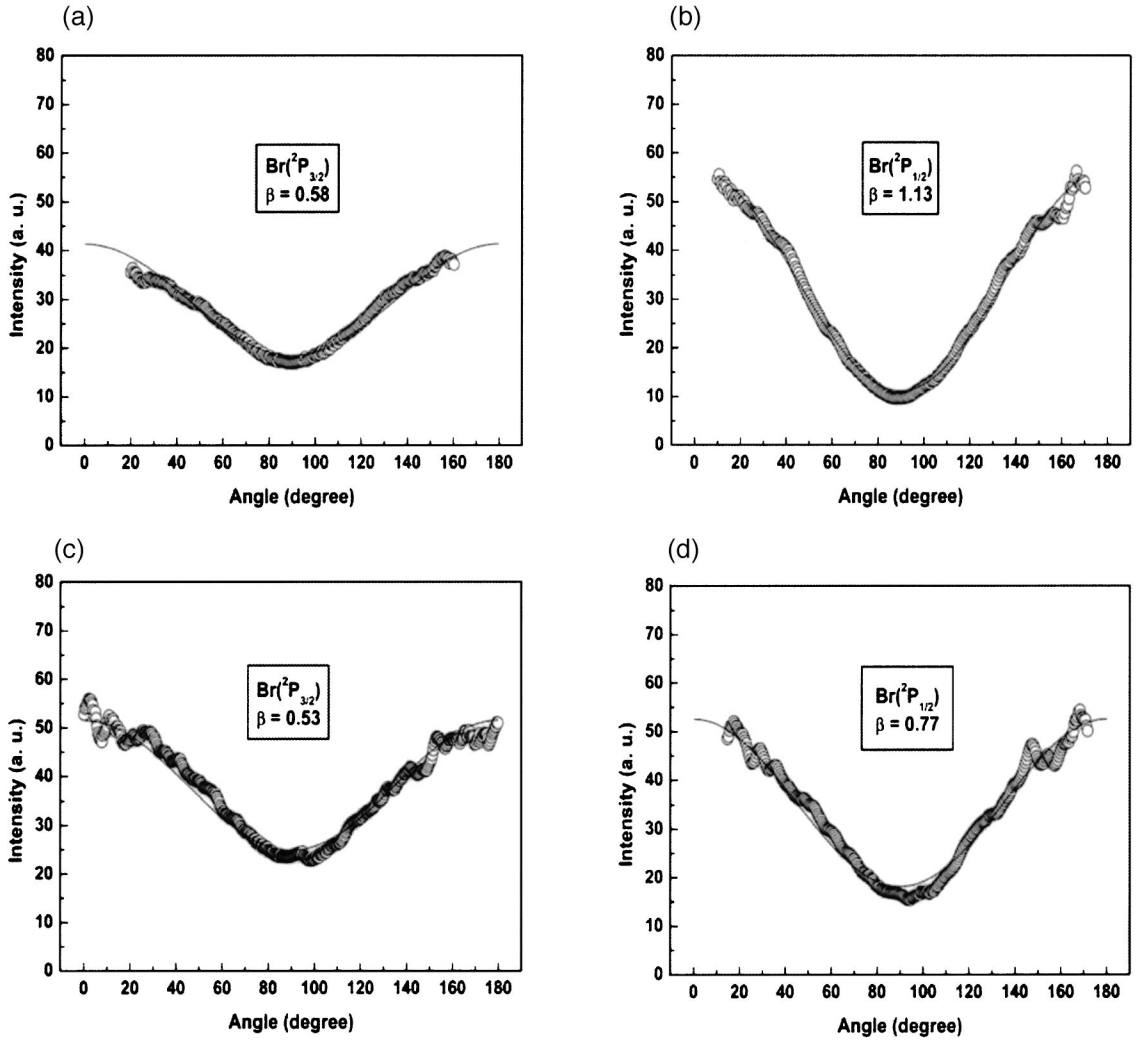

FIG. 2. Overall angular distributions of Br (a) and (c) and Br* (b) and (d) from C_2H_3Br and C_2F_3Br. Each data point represents the signal intensity that has been integrated over an overall range of speed. The open circles are the experimental data and the anisotropy parameters are extracted by the fitted curves (solid lines) using Eq. (1).

$$E_T=\frac{1}{2}(m_{C_2Y_3}+m_{Br})\frac{m_{Br}}{m_{C_2Y_3}}v_{Br}^2, \tag{3}$$

where Y denotes H for C_2H_3Br and F for C_2F_3Br. $P(v)$ is extracted by integrating the reconstructed 3D speed distribution over all angles at each speed. The total translational energy distributions for Br and Br* from C_2H_3Br and C_2F_3Br are plotted in Fig. 3. In the case of Br and Br* from C_2H_3Br, the distributions can be fitted by at least four components. One Boltzmann and three Gaussian distribution patterns were used to obtain the best fit for each distribution. We have also employed prior distributions for the low-energy components[33,34]

$$P(E_T)=AE_T^{1/2}(E_{avl}-E_T)^{s+1/2}/E_{avl}^{s+2}, \tag{4}$$

where A is a normalization constant, E_{avl} the available energy, and s the number of vibrational degrees of freedom of a vinyl radical $(s=3N-6=9)$. The fitted results have shown reasonable agreement with those obtained using Boltzmann distributions. In general, prior distributions can be approximated to Maxwell–Boltzmann distribution formulas taking the limit as $s\rightarrow\infty$[35]

$$\lim_{s\rightarrow\infty} P(E_T)=A'E_T^{1/2}\exp(-E_T/kT). \tag{5}$$

The translational temperatures corresponding to the Boltzmann components have been 2600–3100 K from the best-fit. In order to infer the contribution of each component to recoil anisotropy, β values corresponding to individual translational energy values were extracted and plotted in Fig. 3. β values were found to vary from -0.26 to 1.06 in the case of Br and from 0.20 to 1.29 in the case of Br*, respectively. On the other hand, the recoil anisotropy distributions for Br and Br* from C_2F_3Br varied from -0.35 to 0.92 and from 0.30 to 0.97, respectively.

The average translational energies for individual Gaussian components have been determined and denoted as $\langle E_T\rangle_{Gs}^{low}$, $\langle E_T\rangle_{Gs}^{middle}$, and $\langle E_T\rangle_{Gs}^{high}$. They are listed in Table I. The available energy, E_{avl}, was calculated by

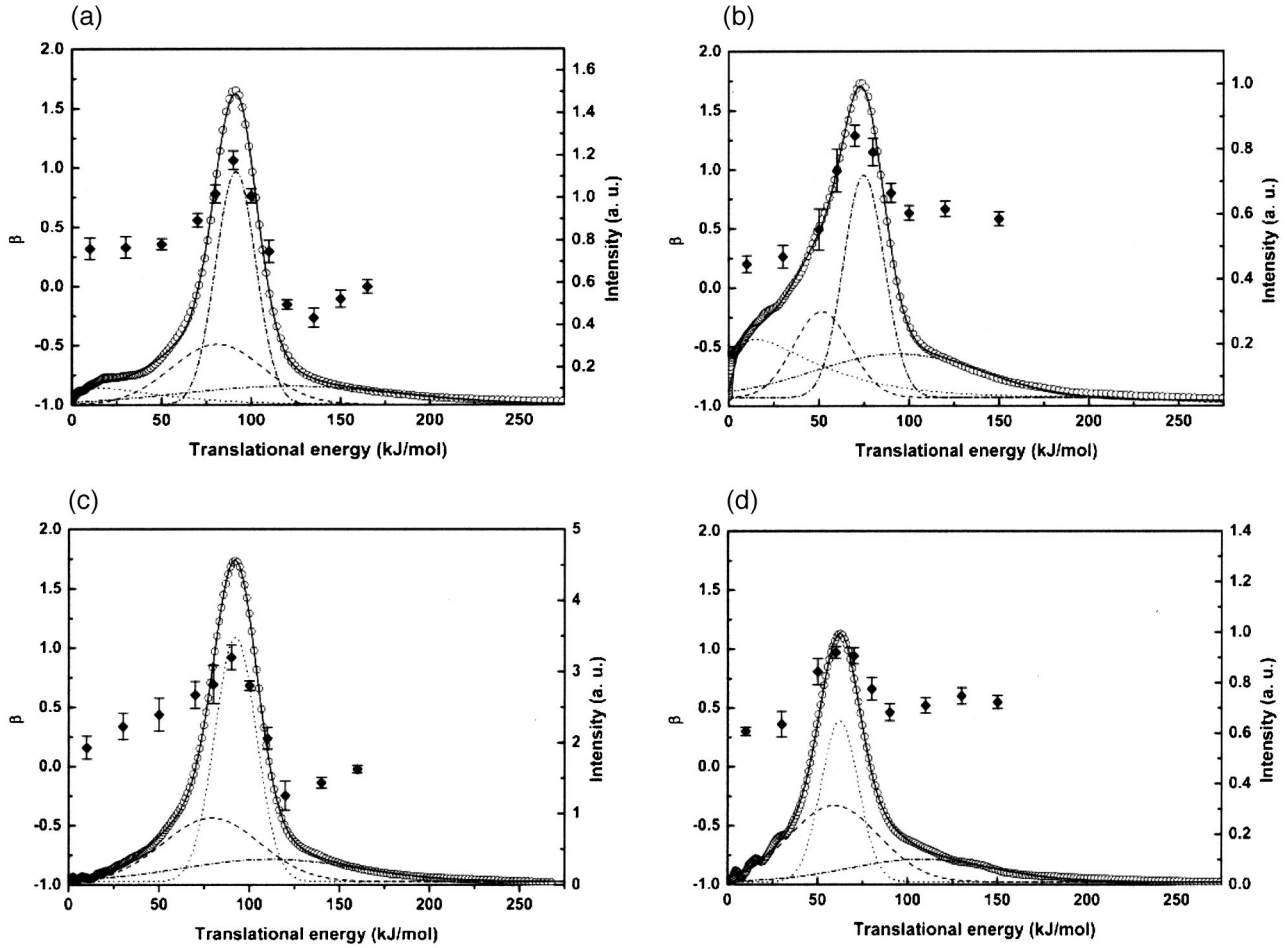

FIG. 3. Total translational energy distributions of Br (a) and (c) and Br* (b) and (d) from C_2H_3Br and C_2F_3Br. Each data point (open circle) corresponds to the relative signal intensity (in arbitrary units as shown in the axes on the right) obtained by integrating values for all angular components at a specific translational energy. The anisotropy parameters as a function of the translational energy are shown as filled diamonds and the axes on the left. In (a) and (b), the dotted lines (· · · ·) show statistical distributions. In all figures, the low Gaussian components are denoted by dashed lines (— — —). The dash–dot lines (—·—·—·—) and the dash–dot–dot lines (—··—) correspond to the middle and high Gaussian components, respectively. The solid lines (——) represent the linear combinations of individual components.

$$E_{\mathrm{avl}} = E_{h\nu} - D_0 - E_{el} + E_{\mathrm{int}}, \tag{6}$$

where $E_{h\nu}$, D_0, E_{el}, and E_{int} represent the photon energy, the dissociation energy of C–Br, the electronic energy of Br atoms, and the internal energy of a parent molecule, respectively. From the literature, $D_0 = 331.3$ kJ/mol was obtained for C_2H_3Br.[36,37] $E_{el} = 0$ and 43.9 kJ/mol, generally accepted values, were used for Br and Br*, respectively. E_{int} was assumed to be zero in the present experimental conditions using a supersonic molecular beam. The fraction of an average translational energy for each component over the available energy, f_T, is listed also in Table I.

TABLE I. The average translational energies and f_T values of the translational energy components of $C_2H_3 + Br(Br^*)$ and $C_2F_3 + Br(Br^*)$ at 234 nm. Only the values for C_2H_3Br are presented because D_0 for C_2F_3Br is not available in literature. Units in kJ/mol.

Channels	E_{avl}	$\langle E_T \rangle_{\mathrm{Gs}}^{\mathrm{low}}$	$\langle E_T \rangle_{\mathrm{Gs}}^{\mathrm{middle}}$	$\langle E_T \rangle_{\mathrm{Gs}}^{\mathrm{high}}$	$f_{T\,\mathrm{Gs}}^{\mathrm{low}}$	$f_{T\,\mathrm{Gs}}^{\mathrm{middle}}$	$f_{T\,\mathrm{Gs}}^{\mathrm{high}}$
$C_2H_3 + Br$	179.5	74.6	90.5	107.1	0.42	0.50	0.60
$C_2H_3 + Br^*$	136.2	49.0	74.2	81.5	0.36	0.55	0.60
$C_2F_3 + Br$		80.2	93.5	101.8			
$C_2F_3 + Br^*$		51.3	70.9	93.3			

The relative quantum yields of Br and Br* were extracted from relative signal intensities in TOF spectra

$$N_{\mathrm{Br}^*}/N_{\mathrm{Br}} = kI_{\mathrm{Br}^*}/I_{\mathrm{Br}}, \tag{7}$$

$$\Phi_{\mathrm{Br}} = \frac{N_{\mathrm{Br}}}{N_{\mathrm{Br}} + N_{\mathrm{Br}^*}} = (1 + N_{\mathrm{Br}^*}/N_{\mathrm{Br}})^{-1}, \tag{8}$$

$$\Phi_{\mathrm{Br}^*} = \frac{N_{\mathrm{Br}^*}}{N_{\mathrm{Br}} + N_{\mathrm{Br}^*}} = \frac{N_{\mathrm{Br}^*}}{N_{\mathrm{Br}}}(1 + N_{\mathrm{Br}}/N_{\mathrm{Br}^*})^{-1}, \tag{9}$$

where N_X and I_X (X=Br and Br*) designate the number and the measured signal intensity of the species X, respectively. The parameter k is related to REMPI probability ratios, detection efficiencies, and other instrumental factors. k was found to be 0.42 under the present experimental conditions. For C_2H_3Br, $I_{\mathrm{Br}^*}/I_{\mathrm{Br}}$ was measured to be 0.17 ± 0.01 and $N_{\mathrm{Br}^*}/N_{\mathrm{Br}}$ is 0.071 ± 0.004. The resultant relative quantum yields are $\Phi_{\mathrm{Br}} = 0.93$ and $\Phi_{\mathrm{Br}^*} = 0.07$. In the case of C_2F_3Br,

TABLE II. The relative quantum yields and the branching ratios of the translational energy components of $C_2H_3+Br(Br^*)$ and $C_2F_3+Br(Br^*)$ at 234 nm.

Channels	Φ_{Bz}	Φ_{Gs}^{low}	Φ_{Gs}^{middle}	Φ_{Gs}^{high}	Φ_{total}
C_2H_3+Br	0.05±0.01	0.29±0.05	0.41±0.02	0.18±0.03	0.93
$C_2H_3+Br^*$	0.013±0.001	0.014±0.002	0.024±0.001	0.019±0.001	0.07
Br^*/Br	0.26	0.048	0.059	0.11	0.07
C_2F_3+Br	···	0.28±0.03	0.43±0.01	0.20±0.02	0.91
$C_2F_3+Br^*$	···	0.040±0.004	0.025±0.004	0.025±0.003	0.09
Br^*/Br	···	0.14	0.058	0.13	0.10

$I_{Br^*}/I_{Br}=0.24\pm0.08$ and N_{Br^*}/N_{Br} is determined to be 0.10 ±0.03. The relative quantum yields are $\Phi_{Br}=0.91$ and $\Phi_{Br^*}=0.09$. Based on these values, the relative quantum yields for individual energy components in Fig. 3 were obtained and listed in Table II.

IV. DISCUSSION

In the 234 nm photodissociation of C_2H_3Br, the translational energy distributions of Br and Br* were fitted well by a single Boltzmann function and three Gaussian functions. On the other hand, no Boltzmann distribution function was required to fit the distributions of Br and Br* from C_2F_3Br, but only three Gaussian functions were used. Since each component stems from one or more processes, at least 4 dissociation routes must be considered in order to identify the origins of individual components. Energetically possible primary and secondary processes leading to the formation of Br and Br* are

$$C_2H_3Br \rightarrow C_2H_2+HBr \rightarrow C_2H_2+H+Br(^2P_j) \quad \text{(a)}$$

$$\rightarrow C_2H_3Br^{**} \rightarrow C_2H_3(\tilde{A})+Br(^2P_j) \quad \text{(b)}$$

$$\rightarrow C_2H_3(\tilde{X})+Br(^2P_j). \quad \text{(c)}$$

In the case of the molecular elimination channel (a), energy that can be distributed to the recoil energy of Br atoms can be estimated by

$$E_T(Br)=\frac{m_H}{m_{HBr}}\{E_{h\nu}+E_{int}(HBr)-D_0(H\text{-}Br)-E_{el}(Br)\}, \quad (10)$$

where the photon energy, $E_{h\nu}$, and the dissociation energy of HBr, $D_0(H–Br)$, are 511 and 361.9 kJ/mol, respectively. The electronic energies, E_{el}, of Br and Br* are 0 and 44 kJ/mol, respectively. The internal energy of HBr, $E_{int}(HBr)$, is obtained from the literature. In a study on the molecular elimination of C_2H_3Br at 193 nm, vibrational levels of HBr higher than $v=7$ have not been observed.[38,39] Accordingly, the internal energy of HBr, $E_{int}(HBr)$, is presumably less than 167.3 kJ/mol. The translational energies of Br and Br* cannot exceed 4 kJ/mol. The molecular elimination (a), hence, should be eliminated from the production channel of Br and Br* in present study.

In the case of channel (b), the available energy, E_{avl}, were estimated to be −60.1 and −104.0 kJ/mol for Br and Br*, respectively. The energy level of the (0,0) band of the $\tilde{X}\rightarrow\tilde{A}$ transition in C_2H_3 radical was chosen to be 239.8 kJ/mol referring to a work using cavity ring-down spectroscopy.[40] C–Br bond dissociation energy, D_0, was determined to be 331.3 kJ/mol from the value of a pulsed field ionization-photoelectron-photoion coincidence method[37] and G2 theory.[36] In this, the negative available energies indicate that the channel (b) is not plausible.

The channel (c) seems to be the only channel generating Br and Br* observed in this work. Although some C_2H_3Br dissociation dynamics are reported, there still exist the controversy on exact dissociation pathways. In a 193 nm C_2H_3Br study, it was attempted to use a Boltzmann and a Gaussian distribution to explain the translational energy distributions of fragments and suggested that the former stems from an internal conversion process.[27,29] In the latter case, curve-crossing from a bound excited state [originating from $^1(\pi,\pi^*)$ transition localized on C=C bond] to a repulsive state was proposed. Both ideas are based on the analogy between the two systems, C_2H_3Br and C_2H_3Cl. However, it should be mentioned that there are also controversies on the exact photodissociation dynamics of chlorinated ethylene systems.

In the *ab initio* configuration interaction calculation by Michl and Bonacic-Koutecky[41] and by Mains *et al.*,[28] $^3A'(\pi,\pi^*)$, $^3A''(\pi,\sigma^*)$, $^1A''(\pi,\sigma^*)$, and $^3A'(n,\sigma^*)$ states can be reached at 193 nm (~511 kJ/mol). $^1A'(n,\sigma^*)$ in Fig. 4 lies much higher than the photon energy and its contribution to the photodissociation can be ignored. $^3A'(\pi,\pi^*)$ is the lowest-lying state[28] and expected to have a barrier into the exit channel. The lowest energy Gaussian component in each plot has been ascribed to the predissociation via $^3A'(\pi,\pi^*)$. The broad energy distribution and the recoil anisotropy parameter less than the limit value (Fig. 3) coincide with the result by *ab initio* calculation where an energy barrier in the exit channel is expected.

The $^3A''(\pi,\sigma^*)$ and $^1A''(\pi,\sigma^*)$ states lie above $^3A'(\pi,\pi^*)$.[28] They arise from the promotion of a lone-pair π electron on Br onto a σ^* orbital. They are responsible to the middle translational energy component. These two states are nearly equal in energy and have little difference in the asymptote region. It is thus difficult to discern which of them contributes more in detail.[28] As shown in Fig. 3, this middle energy component is characteristic of a parallel transition. The anisotropy parameter reaches maximum in every case at the center of the profile of this component. For example, in the case of Br from C_2H_3Br, β reaches 1.06. Katayanagi *et al.* obtained similar value ($\beta=1.2$) for the 193 nm photodissociation of C_2H_3Br. They have estimated that the direction of the transition dipole moment is tilted by 31.1° with respect to the C–Br bond based on their data and suggested

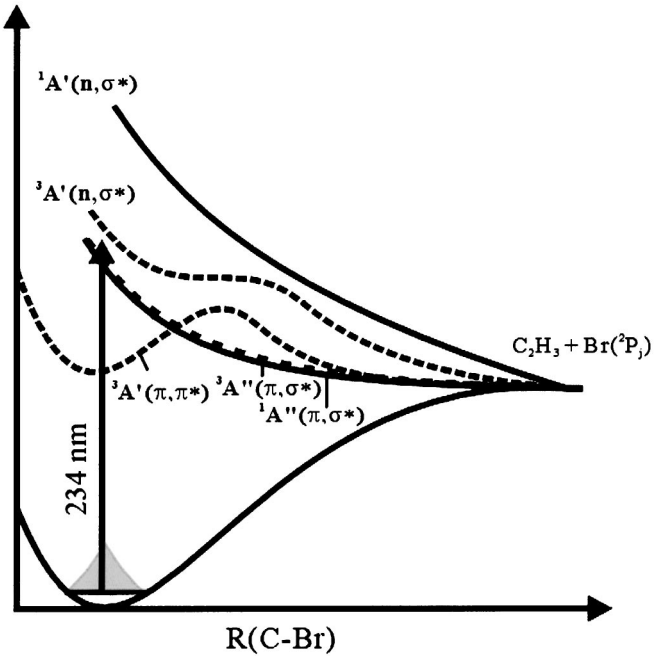

FIG. 4. Schematic diagram representing *ab initio* CI potentials for vinyl bromide from Refs. 28 and 36.

that prompt dissociation occurs within a rotational period.[29]

The highest accessible state, $^3A'(n,\sigma^*)$, has an energy barrier that indicates the interactions with other nearby states and suggests to be the origin of the highest Gaussian component. The broad profile and low anisotropy parameter agree with the energy barrier in the exit channel.

In Figs. 3(a) and 3(b), Boltzmann components have been observed in C_2H_3Br photolysis. Similar shaped-profiles have also been found as well as the multi-modal translational energy distributions of Cl in chlorinated ethylenes and allyl chloride.[14,15,17,19–21,42,43] These findings have been interpreted as an indication that the origin of the statistical component relies on the internal conversion from the initially excited $^1(\pi,\pi^*)$ state, a bound state, to the vibrationally excited ground state.[14,15,17,19–21,42,43]

It is general believe that the excited singlet $^1(\pi,\pi^*)$ state is a turning point to various dissociation channels for chlorinated ethylenes and allyl chloride UV photoreactions. Earlier reported energy level of this state varies from 6.65 to 7.8227 eV with calculation levels and methods used.[18,20,44] A recent study proposed triplet states as the responsible state for the excitation of C_2H_3Cl since the $^1(\pi,\pi^*)$ state lies too high to be involved.[44] The energy levels of triplet states are 3.4–5.1 eV by low energy electron-impact energy-loss spectroscopy.[45] Therefore, it seems reasonable that the Boltzmann component results not from internal conversion but from intersystem crossing followed by the triplet states excitation.

In the absorption spectrum of C_2H_3Br, an absorption maximum near 200 nm is attributed to $^1(\pi,\pi^*)$.[25] A shoulder is observed in the long wavelength region, implying that some states other than $^1(\pi,\pi^*)$ are dominant at 234 nm. The absorption spectrum have not been assigned completely yet and so as the physical properties of the excited states of C_2H_3Br have not much known. Nevertheless, we suggest that the $^3A'(\pi,\pi^*)$ state is the major contribution based on the result of Michl *et al.* and Mains *et al.*[28,41] They have shown that $^3A'(\pi,\pi^*)$ lies at ~362.8 kJ/mol above the ground state using a configuration interaction method with single excitation.[28] Excitation to this state weakens the C═C bond, and a torsional motion along the bond axis becomes more probable. In addition, the spin–orbit coupling energy of Br (44 kJ/mol) is four times larger than that of Cl (10.5 kJ/mol). Therefore, the probability for intersystem crossing from $^3A'(\pi,\pi^*)$ to the ground state increases.

On the other hand, the Boltzmann component is absent in the case of C_2F_3Br dissociation. Since F atoms reduce the electron density in the π^* orbital on the C═C bond, the intersystem crossing from the triplet $^3A'(\pi,\pi^*)$ state to the ground state is not as easy as in C_2H_3Br. Effects of fluorination have also been investigated in a study of aryl halide systems.[46–48] By fluorination, the excitation energies of the lowest $\sigma^*\leftarrow\pi$ transition and the triplet $\sigma^*\leftarrow n$ transition in iodobenzene have been lowered, and the $\pi^*\leftarrow\pi$ transition energy increases.[46–48] As a result, mixing of these transitions becomes more probable, implying the contribution of $^{1,3}(\pi,\sigma)$ and $^3(n,\sigma)$ to dissociation becomes larger. In alkyl halides, it has been observed that fluorination reduces the probability of curve crossing between $^3Q_0$ and $^1Q_1$.[12,48]

The branching ratio of Br*/Br=0.07 for C_2H_3Br agrees well with 0.06 obtained in the 193 nm photodissociation of C_2H_3Br. The branching ratio of C_2F_3Br is observed to be Br*/Br=0.10. The branching ratio, 0.07, for C_2H_3Br is different from that of Mains *et al.* based on the statistical model.[28] If the process is purely statistical, the ratio should be 0.5 as same as the ratio of spin-multiplicity, [2(1/2)+1]/[2(3/2)+1]. Even Boltzmann components in the C_2H_3Br photolysis, the ratio, 0.25, cannot be explained by the statistical process alone. The discrepancy indicates that there are some interactions between states in exit channels. At present stage of this study, however, the full mechanism of the interactions is premature to clarify, due to the complications of the system and lack of supporting information. It is deemed necessary, therefore, further study for the complete interpretation.

V. SUMMARY

In the present study, the photodissociation dynamics of vinyl bromide (C_2H_3Br) and perfluorovinyl bromide (C_2F_3Br) have been investigated at 234 nm using a photofragment ion imaging technique with a state-selective REMPI scheme. In the C_2H_3Br, the nascent Br atoms stem from the primary C–Br bond dissociation leading to the formation of $C_2H_3(\tilde{X})$ and $Br(^2P_j; j=1/2,3/2)$. The obtained translational energy distributions were well fitted by a single Boltzmann and three Gaussian functions. Based on the *ab initio* configuration interaction (CI) potential energy surfaces, the lowest energy Gaussian components have been assigned to the predissociation via $^3A'(\pi,\pi^*)$ state. The nearly identical $^3A''(\pi,\sigma^*)$ and $^1A''(\pi,\sigma^*)$ states both in energy and the asymptote region are responsible for the middle translational energy components. The highest acces-

sible $^3A'(n,\sigma^*)$ state has been considered as the origin of the highest Gaussian components. The observed recoil anisotropy and width of the Gaussian functions have also been in accordance with the assignment. It is suggested that the intersystem crossing followed by the excitation to the triplet $^3A'(\pi,\pi^*)$ state to the ground state has been responsible for the Boltzmann component. The weakening of the C═C bond by excitation to this state and a resultant torsional motion make the intersystem crossing probable. The large spin–orbit coupling energy of Br has been considered to increase the probability for the electronic relaxation. In C_2F_3Br photodissociation, the Boltzmann component has not been observed. It is believed that the fluorination reduces the probability for intersystem crossing compared with C_2H_3Br as the electron density in the π^* orbital on the C═C bond is decreased. The branching ratios of Br^*/Br show that the dissociation processes are not statistical. In order to better understand the effect of other chromophore on the photodissociation of organic halide molecules, we are investigating the benzene halides and other molecules having conjugated C═C double bonds.

ACKNOWLEDGMENTS

The authors gratefully acknowledge support from Creative Research Initiation Program of the Korean Ministry of Science and Technology, and School of Molecular Science through the Brain Korea 21 project.

[1] R. K. Sparks, K. Shobatake, L. R. Carlson, and Y. T. Lee, J. Chem. Phys. **75**, 3838 (1981).
[2] M. D. Person, P. W. Kash, and L. J. Butler, J. Chem. Phys. **94**, 2557 (1991).
[3] Y. Amatatsu, S. Yabushita, and K. Morokuma, J. Chem. Phys. **104**, 9783 (1996).
[4] Y. S. Kim, W. K. Kang, D.-C. Kim, and K.-H. Jung, J. Phys. Chem. A **101**, 7576 (1997).
[5] A. T. J. B. Eppink and D. H. Parker, J. Chem. Phys. **110**, 832 (1999).
[6] J. H. Butler, M. Battlet, M. L. Bender, S. A. Montzka, A. D. Clarke, E. S. Saltzman, C. M. Sucher, J. P. Severinghaus, and J. W. Elkins, Nature (London) **399**, 749 (1999).
[7] Y.-J. Jung, M. S. Park, Y. S. Kim, K.-H. Jung, and H.-R. Volpp, J. Chem. Phys. **111**, 4005 (1999).
[8] R. S. Mulliken, J. Chem. Phys. **3**, 514 (1935).
[9] R. S. Mulliken, J. Chem. Phys. **8**, 382 (1940).
[10] A. Gedanken and M. D. Rowe, Chem. Phys. Lett. **34**, 39 (1975).
[11] B. R. Johnson, C. Kittrell, P. B. Kelly, and J. L. Kinsey, J. Phys. Chem. **100**, 7743 (1996).
[12] T. K. Kim, M. S. Park, K. W. Lee, and K. H. Jung, J. Chem. Phys. **115**, 10745 (2001).
[13] M. J. Berry, J. Chem. Phys. **61**, 3114 (1974).
[14] M. Umemoto, K. Seki, H. Shinohara, U. Hagashima, N. Nishi, M. Kinoshita, and R. Shimada, J. Chem. Phys. **83**, 1657 (1985).
[15] Y. Mo, K. Tonokura, Y. Matsumi, M. Kawasaki, T. Sato, T. Arikawa, P. T. A. Reilly, Y. Xie, Y. Yang, Y. Huang, and R. J. Gordon, J. Chem. Phys. **97**, 4815 (1992).
[16] J. Riehl and K. Morokuma, J. Chem. Phys. **100**, 8976 (1994).
[17] Y. Huang, Y. Yang, G. He, S. Hashimoto, and R. J. Gordon, J. Chem. Phys. **103**, 5476 (1995).
[18] P. W. Browning, D. C. Kitchen, M. F. Arendt, and L. J. Butler, J. Phys. Chem. **100**, 7765 (1996).
[19] K. Sato, S. Tsunashima, T. Takayanagi, G. Fujisawa, and A. Yokoyama, J. Chem. Phys. **106**, 10123 (1997).
[20] K. Tonokura, L. B. Daniels, T. Suzuki, and K. Yamashita, J. Phys. Chem. A **101**, 7754 (1997).
[21] D. A. Blank, W. Sun, A. G. Suits, Y. T. Lee, S. W. North, and G. E. Hall, J. Chem. Phys. **108**, 5414 (1998).
[22] P. Farmanara, V. Stert, and W. Radloff, Chem. Phys. Lett. **288**, 518 (1998).
[23] T. L. Myers, D. C. Kitchen, B. Hu, and L. J. Butler, J. Chem. Phys. **104**, 5446 (1996).
[24] M. S. Park, K. W. Lee, and K.-H. Jung, J. Chem. Phys. **114**, 10368 (2001).
[25] J. Schander and B. R. Russell, J. Am. Chem. Soc. **98**, 6900 (1976).
[26] V. L. Orkin, F. Louis, R. E. Huie, and M. J. Kurylo, J. Phys. Chem. A **106**, 10195 (2002).
[27] A. M. Wodtke, E. J. Hintsa, J. Somorjai, and Y. T. Lee, Isr. J. Chem. **29**, 383 (1989).
[28] G. J. Mains, L. M. Raff, and S. A. Abrash, J. Phys. Chem. **99**, 3532 (1995).
[29] H. Katayanagi, N. Yonekuira, and T. Suzuki, Chem. Phys. **231**, 345 (1998).
[30] W. K. Kang, Y. S. Kim, and K.-H. Jung, Chem. Phys. Lett. **244**, 183 (1995).
[31] D. W. Chandler and P. L. Houston, J. Chem. Phys. **87**, 1445 (1987).
[32] A. T. J. B. Eppink and D. H. Parker, Rev. Sci. Instrum. **68**, 3477 (1997).
[33] F. Zamir and R. D. Levine, Chem. Phys. **52**, 253 (1980).
[34] T. Baer and W. L. Hase, *Unimolecular Reaction Dynamics: Theory and Experiments* (Oxford university press, New York, 1996).
[35] K. Tsukiyama and R. Bersohn, J. Chem. Phys. **86**, 745 (1986).
[36] M. N. Glukhovtsev and R. D. Bach, J. Phys. Chem. A **101**, 3574 (1997).
[37] X. M. Qian, K. C. Lau, and C. Y. Ng, J. Chem. Phys. **120**, 11031 (2004).
[38] D.-K. Liu, L. T. Letendre, and H.-L. Dai, J. Chem. Phys. **115**, 1734 (2001).
[39] S.-R. Lin, S.-C. Lin, Y.-C. Lee, Y.-C. Chou, I.-C. Chen, and Y.-P. Lee, J. Chem. Phys. **114**, 7396 (2001).
[40] C. D. Pibel, A. Mcllroy, C. A. Taatjes, S. Alfred, K. Patrick, and J. B. Halpern, J. Chem. Phys. **110**, 1841 (1999).
[41] J. Michl and V. Bonacic-Koutecky, *Electronic Aspects of Organic Photochemistry* (Wiley, New York, 1990).
[42] T. Suzuki, K. Tonokura, L. S. Bontuyan, and N. Hashimoto, J. Phys. Chem. **98**, 13447 (1994).
[43] H. S. Ko, Y. R. Lee, C. C. Chen, L. D. Wang, and S. M. Lin, J. Chem. Phys. **117**, 6038 (2002).
[44] J.-L. Chang and Y.-T. Chen, J. Chem. Phys. **116**, 7518 (2002).
[45] C. F. Koerting, K. N. Walzl, and A. Kuppermanm, Chem. Phys. Lett. **109**, 140 (1984).
[46] J. E. Frietas, H. J. Hwang, and M. A. El-Sayed, J. Phys. Chem. **99**, 7395 (1995).
[47] K. Kavita and P. K. Das, J. Chem. Phys. **112**, 8426 (2000).
[48] D. Ajitha, D. G. Fedorov, J. P. Finley, and K. Hirao, J. Chem. Phys. **117**, 7068 (2002).